DESIGN AND OPTIMIZATION OF A TESLA PUMP FOR ORC APPLICATIONS

E.P. Anselmi[1], D. Fiaschi[2], G. Manfrida[2], G. Nicotra[2], L. Talluri[2*]

[1]Cranfield University, Department or Equivalent, City, State, Country

[2] Department of Industrial Engineering, University of Florence, Viale Morgagni 40-44, Italy

*Corresponding Author: lorenzo.talluri@unifi.it

ABSTRACT

The Tesla pump is bladeless turbomachinery known for being more resistant to work with hard-to-pump fluids than conventional turbomachinery, thanks to its simple, robust mechanical design and its working principle (viscous forces).
A 2D numerical model is developed and a design procedure of a Tesla pump working with several working fluids (water, R1233zd(E), R1234yf) is proposed. A complete design methodology is developed by evaluating the losses of each component and by introducing a rotor model. The main optimizing parameters of the pump are highlighted and assessed and validation of the model with available experimental results is carried out.
A design procedure for a Tesla pump prototype is showed and its characteristic curves are obtained and discussed. The results achieved are similar to other experimental Tesla pumps, with a maximum achieved efficiency of 26.8%. The extension of the model to organic working fluids allowed to predict pump efficiencies higher than 50% for low mass flow rate conditions for both assessed fluids.

1 INTRODUCTION

In the early days of its invention, the Tesla pump was regarded mainly as a conceptual design due to issues in efficiency compared to traditional bladed turbomachinery. In the 1950s, the interest renewed about the characteristic of flow between rotating discs, and many studies were performed to further understand the phenomenon. But the interest has waned again in the 1970s because, despite the efficiency of the tesla turbomachinery was improved, the bladed turbomachinery efficiency was still much higher. In the early 2000s, the interest in Tesla turbomachinery came back and today there are some applications where the Tesla pump could be useful (Rice, 1963).
A Tesla pump consists of smooth, co-axial parallel discs on a drive shaft, arranged such that there are small spaces between the discs. The rotor is placed inside a casing with small radial and axial clearance. The fluid enters the pump rotor through the holes or slots near the shaft and leaves the pump through a volute/diffuser located in the pump casing. In the Tesla pump, the pumping does not impinge on the rotating pump mechanism, so that it generates a pulsation-free, laminar flow pattern through the pump (Pacello and Hanas, 2000). This type of pump has also a low susceptibility to cavitation and can run at very high angular velocities. Thanks to these characteristics the Tesla pump is a strong alternative in hard-to-pump applications, such as pumping highly abrasive slurries, viscous slurries, slurries with a high solids content, fluids with entrained air, and fluids containing delicate or shear sensitive products. Another important advantage is that the pump has a lower sensitivity to cavitation compared to other pump types. Studies about the Tesla pump showed also that could be very useful in pumping blood because the working principle of the pump allows keeping well the blood quality when pumped (Foster, 2006). Besides, it can be used with compressible fluids, in that case, it works as a compressor. The most interesting applications in this field are the supercritical fluids, as CO_2 (Brun et al., 2017), which, thanks to their high density, allow to reduce the turbomachinery size as fewer compression and expansion stages are required. Thus, the compressor work would be reduced obtaining a higher useful work and

consequently, increasing the thermal efficiency. The use of supercritical fluids in Tesla turbomachinery could improve the low efficiency of this turbomachine. Another possible solution to increase efficiency is to optimize the geometry of the rotor not utilizing straight channels, but slightly curved (Alonso et al., 2019)

The biggest issue that blocked the Tesla pump to take up an important position on the market is the very low efficiency compared with the conventional pumps. Table 1 resumes the pumps available on markets, as well as the advantages and disadvantages of each technology, compared to the Tesla pump. The aim of this research is therefore to develop and validate an analytical model capable to predict the performance of the Tesla pump working with water and extending the developed model to predict the performance when organic fluids are employed.

To reach this result the following step objectives must be satisfied:

1. Develop an analytical model able to calculate the performance of the Tesla pump;
2. Validate the model results against experimental data found in the literature;
3. Design of a Tesla pump prototype working with water;
4. Parametric analysis of the prototype performance.
5. Extension of the model to organic fluids.

Table 1: Pumps type general characteristics (Pacello and Hanas, 2000, Foster, 2006)

Type	Flow rate [m^3/h]	Head [m]	Efficiency	Cost	Characteristics
Axial-flow pump	> 1000	< 10	< 0.9	high	+ Efficiency, continuous flow - Head, cost, NPSH
Centrifugal pump	< 12000	60 ÷ 100	< 0.75	medium	+ Efficiency, continuous flow, head range - NPSH, high viscous fluid
Positive displacement pump	< 1000	> 100	< 0.97	medium	+ Efficiency, NPSH - flow rate, discontinuous flow
Tesla pump	< 1100	< 300	< 0.5	low	+ NPSH, life, simple design, versatility - efficiency

2 Methodology

The Tesla pump described and analysed in this work consists of several components: a bladeless rotor composed of parallel thin discs fixed to the rotating shaft, a volute external casing, inlet, and exit rotor-ducts connections.

2.1 Rotor model

The rotor model was adapted from (Talluri et al., 2018, Manfrida and Talluri 2019), where it was developed and validated when the Tesla turbomachinery acts as a turbine.

When developing the rotor model, the following assumptions were made:

- Steady and laminar flow
- Body forces negligible compared to viscous forces (viscous flow):
- Two-dimensional flow:
  - $v_z = 0$
  - v_r = constant across the channel
  - v_θ = constant across the channel
- Radial symmetric flow field, uniform at the inlet ($r = r_i$). The flow field is thus the same for any θ, therefore the derivative $\frac{\partial}{\partial \theta} = 0$ for all flow variables

- $\partial p/\partial \theta$ negligible compared to wall friction forces

Flow equations

The fundamental Navier-Stokes equations in cylindrical coordinates are reduced to:

Continuity: $$\frac{1}{r}\frac{\partial(r\rho w_r)}{\partial r} = 0 \quad (1)$$

Momentum, r-direction $$w_r\frac{\partial w_r}{\partial r} - \Omega^2 r - 2\Omega w_\theta - \frac{w_\theta^2}{r} = -\frac{1}{\rho}\frac{\partial p}{\partial r} + \frac{\upsilon\,\partial^2 w_r}{\partial^2 z} \quad (2)$$

Momentum, θ-direction $$w_r\frac{\partial w_\theta}{\partial r} + \frac{w_r w_\theta}{r} + 2\Omega w_r = \frac{\upsilon\,\partial^2 w_\theta}{\partial^2 z} \quad (3)$$

Momentum, z-direction $$\frac{\partial p}{\partial z} = 0 \quad (4)$$

This model introduces an axial velocity profile, assuming that the velocity profile of the fully developed flow was laminar, thus parabolic, so the relative velocities in r and θ directions can be expressed as:

$$w_r(r,z) = \overline{w_r}\, a\, \frac{z}{b}\left(1-\frac{z}{b}\right) \quad (5)$$

$$w_\theta(r,z) = \overline{w_\theta}\, a\, \frac{z}{b}\left(1-\frac{z}{b}\right) \quad (6)$$

Integrating the differential form of the r and θ momentum equations between $z = 0$ and $z = \frac{b}{2}$, and assuming the maximum velocity value at mid-channel and zero velocity at the walls, the equations of the motion are obtained:

r-direction $$\frac{1}{\rho}\frac{dp}{dr} = -\frac{a^2}{30}w_r\frac{\partial w_r}{\partial r} + \Omega^2 r + \frac{a}{6}2\Omega w_\theta + \frac{a^2}{30}\frac{w_\theta^2}{r} - \frac{2a}{b^2}\upsilon w_r \quad (7)$$

θ-direction $$\frac{\partial w_\theta}{\partial r} = -\frac{10}{a}\Omega - \left(\frac{60\upsilon}{w_r b^2 a} + \frac{1}{r}\right)w_\theta \quad (8)$$

High values of the coefficient "a" determine pronounced parabolic distributions, typical of fully developed laminar flows, while low values of a are related to transitional and not fully developed laminar flows, characteristic of the entry region.

2.2 Volute model

The volute shape considered in the present work is a logarithmic spiral. The parameters of the spiral are showed in Fig. 1 and the equation of the spiral is:

$$r_\theta = r_{start}e^{\theta * tg(\alpha_v)} \quad (9)$$

The design concerns the choice of the start radius of the volute r_{start} and the angle α_v that decides the increasing of the radius r_θ at every θ. In this case, the angle θ goes from 0 to 2π. The α_v value that minimised the losses was defined with parametric analysis. The flow direction and velocity at the inlet of the volute were the main parameters that influenced α_v.

$$r_\theta(0) = r_{start} \qquad r_\theta(2\pi) = r_{end} \quad (10)$$

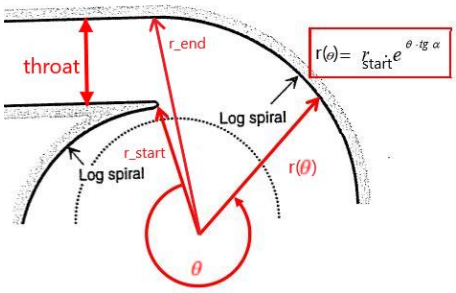

Figure 1: Volute geometry parameters

2.3 Losses

The model takes into account three different types of losses: radial velocity dump losses; friction losses; tangential velocity dump losses.
The calculation of the losses was obtained with the equations suggested by Van den Braembussche, 2006, reported in Eqns. (11-15).

Radial velocity dump losses:
$$\Delta p_{rdl} = \frac{\rho v_{r2}^2}{2} \tag{11}$$

Friction losses:
$$\Delta p_f = f \frac{L}{D_h} \frac{\rho \overline{v_t^2}}{2} \tag{12}$$

Where the friction coefficient f for smooth pipes can be calculated by the Blasius equation:
$$f = 0.3164\ Re^{0.25} \tag{13}$$

The volute channel length L is given by:
$$L = \left(\frac{r_{end}}{\tan(\alpha_v)} - \frac{r_{start}}{\tan(\alpha_v)} \right) \sqrt{1 + \tan^2(\alpha_v)} \tag{14}$$

Tangential velocity dump losses:
$$\Delta p_{tdl} = \gamma_t \frac{\rho (v_{t2} - v_{t3})^2}{2} \tag{15}$$

Where a value of $\gamma_t = 0.5$ is suggested in (Van den Braembussche, 2006).

3 Validation of results

To understand the accuracy of the model performance prediction, a comparison between the model results and experimental results made in (Dodsworth, 2016) has been carried out.
Unfortunately, not all the pump geometry characteristics required by the model were reported in Dodsworth's work, then the dimensions of the outer radius of the volute (or the angle α_v) and the inlet and exit pump pipes diameters were assumed to perform the analysis at 27.5 mm (α_v=3.187°), 32 mm and 32 mm, respectively. The characteristics of Dodsworth's prototype are shown in Table 2.

Table 2: Dodsworth's prototype Tesla pump dimensions and working conditions, with water as working fluid *(Dodsworth, 2016)*.

Rotor disc outer diameter [mm]	**Rotor disc inner diameter [mm]**	**Discs thickness [mm]**	**Channel width [mm]**	**Number of discs**
35	9.5	0.8	0.254	18
Volute shape	**Min gap between rotor and volute [mm]**	**Rotor length [mm]**	**Revolution per minute [rpm]**	**Volumetric flow rate [$\frac{l}{min}$]**
Logarithmic spiral	1.6	20	2500÷ 3600	0.12÷1.53

Figure 2 displays the comparison between the developed model results and the experimental data taken from (Dodsworth, 2016). The model prediction is close to the experimental results. The maximum difference between model and test results was 8.3%, instead, the average results difference was 4.2%. This difference could be imputed to the geometric assumptions used in the model because not all the geometric parameters required by the model were given in the description of the prototype and also it could be due to the accuracy of the instruments of measure.

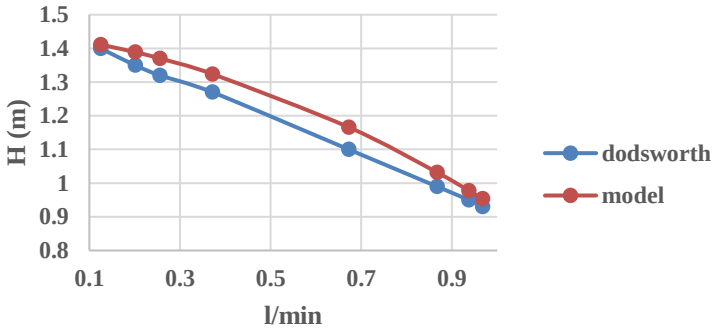

Figure 2: Comparison of model predictions and experimental data provided in *(Dodsworth, 2016)*

4 Results

4.1 Prototype Design

The final prototype geometry was obtained taking into account various aspects. First, a thermodynamic optimization was carried out, then a mechanical analysis was performed of the optimal thermodynamic configuration found. Finally, the manufacturing processes and the restrictions of the test bench available at Cranfield University were taken into account to get the final design. These constraints mainly affected the rotor and volute design. The width and the maximum radius of the discs were limited by the aluminium pieces available in the University facilities. The volute spiral and the junction between the volute and the exit pump pipe were also designed to be manufactured with the tools available at the University. The abrupt change of section between volute and pump exit pipe affected the performance of the pump introducing higher losses. For the sake of brevity, the final dimensions of the prototype are resumed in Tables 3 and 4 and figure 3 presents the assembled scheme of the pump, while in the next subsection the performance maps of the prototype are presented.

Table 3: Rotor dimensions

Rotor inner diameter $[m]$	Rotor outer diameter $[m]$	Channel width $[m]$	Disc thickness $[m]$	Material	Number of discs
0.023	0.076	0.0003	0.0012	Aluminum	25

Table 4: Volute dimensions

R_{in} $[mm]$	R_{out} $[mm]$	α_v [°]	Width $[mm]$	Material
39	52.5	2.635	37.8	Aluminium

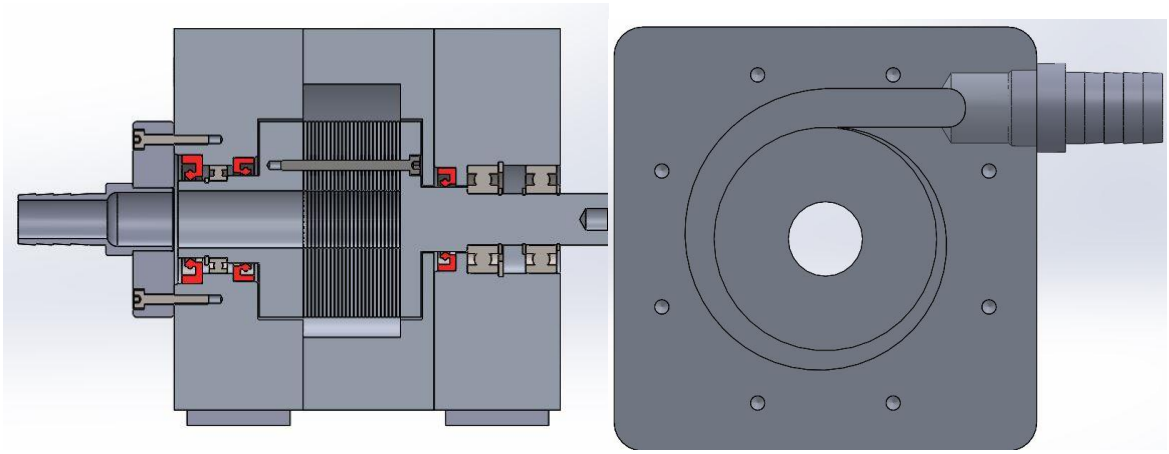

Figure 3: Assembled schematic of the prototype of the Tesla pump

4.2 Performance maps

Figure 4(a) shows the curves of pressure ratio as a function of flow rate at several rotational speeds. As expected, the pressure ratio is higher at a low mass flow rate and higher rotational speeds. The maximum pressure ratio obtained was 2.62, at 5000 rpm, and for a channel width of 0.3 mm.

Figure 4(b) presents the curves of power required as a function of flow rate at several rotational speeds. The power calculation was performed through the sum of the torque multiplied by the angular velocity and the power losses given by the seals in function of the circumferential speed of the shaft. Higher power is required at higher rotational speeds and mass flow rates. The maximum power required was found to be 699.2 W, for 5000 rpm.

The rotor isentropic efficiency as a function of flow rates and rotational speeds are presented in Fig. 5(a). The rotor efficiency trend is very similar to the pressure ratio trends, with higher efficiencies at low mass flow rates and higher rotational speed. The maximum calculated rotor isentropic efficiency was 72.6%, obtained at 5000 rpm. Finally, figure 5(b) displays the efficiency of the whole pump, comprising of the losses effects. It is interesting to note that there is a maximum at each rotational speed and this maximum is present at a higher mass flow rate when higher rotational speeds are considered. The maximum overall pump efficiency obtained was 26.8%, at 5000 rpm.

When increasing the rotational speed from 1000 rpm to 5000 rpm, the energy transmitted by the discs to the fluid increases; furthermore at low rpm the pump could not provide the maximum flow rate settled in the model but could only work until a lower maximum flow rate. For the same reason, the maximum pressure ratio was achieved at higher rpm and lower flow rates.

The performance maps obtained in this work are coherent with the ones reported in (Pacello and Hanas, 2000), which highlights the peculiar pressure ratio and efficiency curves. Indeed, when compared to a "standard" centrifugal pump, the decrease in pressure ratio is greater increasing the mass flow rate, as well as the efficiency which tends to have its maximum at lower mass flow rates. Therefore, it is interesting to note that this kind of pump is prone to be utilized in any application that requires low mass flow rates.

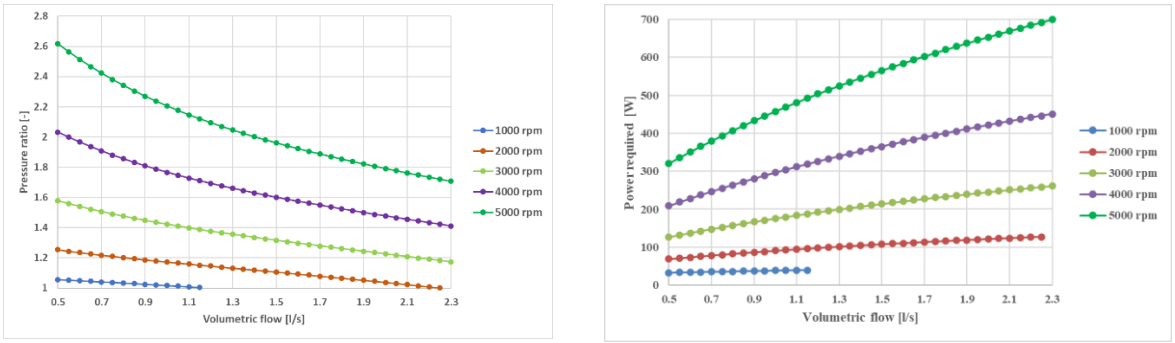

Figure 4: (a) Pressure ratio and (b) required power, as function of mass flow rate and rotational speed.

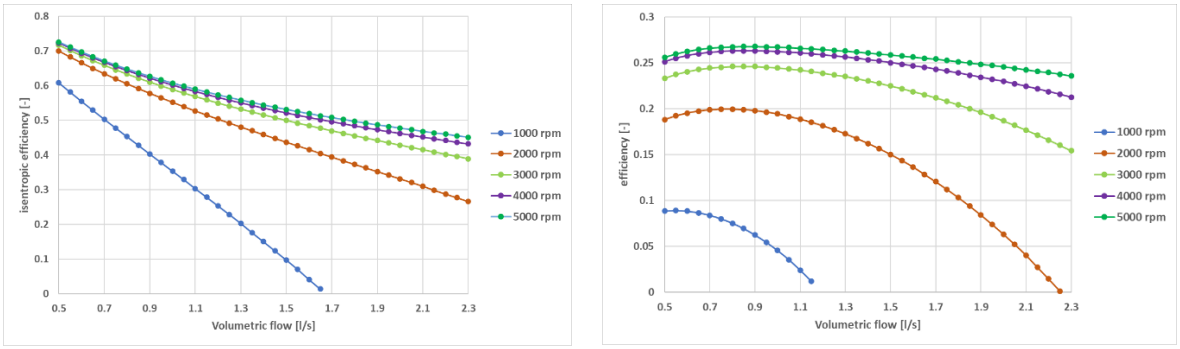

Figure 5: (a) Rotor isentropic efficiency and (b) pump efficiency, as a function of mass flow rate and rotational speed.

4.3 Extension to Organic fluids

The analyses were carried out to simulate significant pressure ratios (e.g. with a difference between evaporator and condenser saturation temperature between 90 and 40°C); therefore, the pump model was run with the geometry defined in Table 5.

Table 5: Pump dimensions

Rotor inner diameter [m]	Rotor outer diameter [m]	Channel width [m]	Disc thickness [m]	α_v [°]	Number of discs
0.016	0.2	0.0003	0.0012	8	50

The inlet pump pressure of the fluids was taken by the condition of saturated liquid referred to 40° C condensation temperature for both fluids: R1233zd(E) and R1234yf, which are new low GWP fluids used in organic Rankine cycles.

4.4 Geometry assessment

In order to properly select the geometry of the pump, parametric analyses of the main parameters were carried out for both fluids.

Particularly, Figure 6 presents the power and efficiency of the pump as a function of (a) d_{ratio} and (b) channel width for R1233zd(E). As can be noted from Fig. 6, power is not affected by diameter ratio, while slightly impact efficiency. A smaller diameter ratio allows a better conversion of the work. On the other hand, the channel width is a fundamental parameter when considering turbine efficiency. Lower diameters are preferred in order to have a high pump efficiency, nonetheless, this comes with a drawback, of a higher power required.

Figure 7 is analogous to Fig. 6, but with R1234yf as the working fluid. The trend displayed is the same as for R1233zd(E).

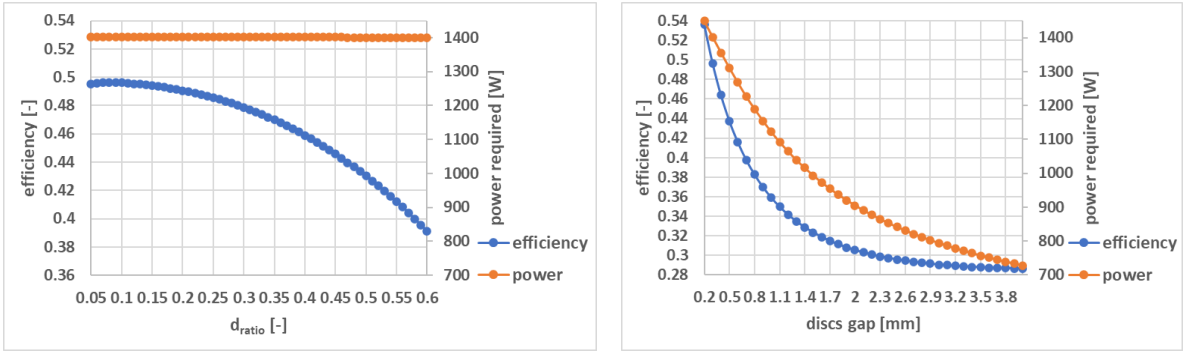

Figure 6: Isentropic efficiency and power as a function of (a) d_{ratio} (b) channel width for R1233zd(E).

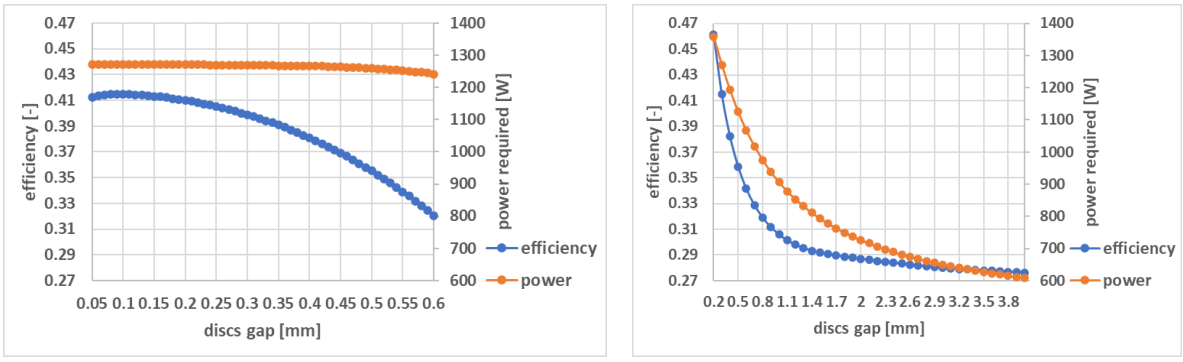

Figure 7: (a) Isentropic efficiency and power as a function of (a) d_{ratio} (b) channel width for R1234yf.

R1233zd(E):

Figure 8(a) shows the curves of pressure ratio as a function of flow rate at several rotational speeds. As for the simulated water cases, the pressure ratio is higher at low mass flow rates and higher rotational speeds. The maximum pressure ratio obtained was 16.36, at 6000 rpm, for a channel width of 0.3 mm. The maximum overall pump efficiency obtained was 56.5%, at 6000 rpm with a mass flow of 0.5 kg/s. Figure 8(b) presents the curves of power required as a function of flow rate at several rotational speeds. The power calculation was performed through the sum of the torque multiplied by the angular velocity and the power losses given by the seals in function of the circumferential speed of the shaft. Higher power is required at higher rotational speeds and mass flow rates. The maximum power required was found to be 7967 W, for 6000 rpm and a mass flow rate of 2.3 kg/s.

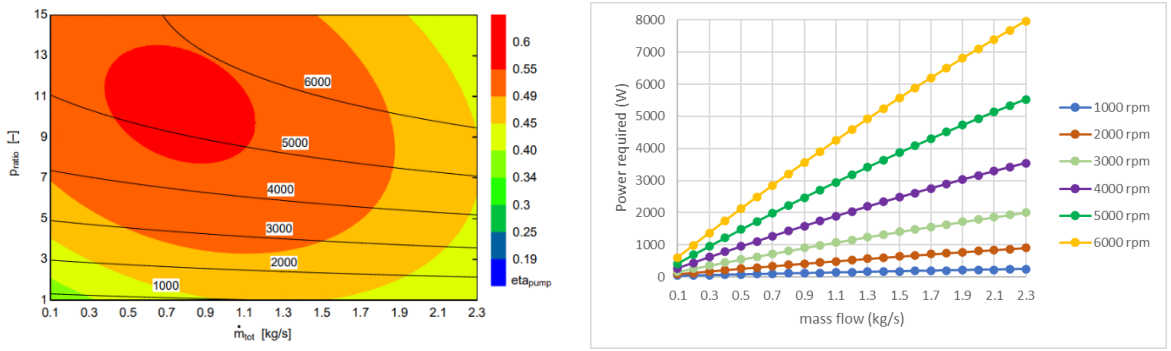

Figure 8: (a) Pressure ratio (black curves) and pump efficiency (colour map); (b) required power, as a function of mass flow rate and rotational speed.

R1234yf:

Figure 9(a) shows the curves of pressure ratio as a function of mass flow rate at several rotational speeds. As for the previous case with R1233zd(E), the pressure ratio is higher at low mass flow rates and higher rotational speeds. The maximum pressure ratio obtained was 3.69, at 6000 rpm, and for a channel width of 0.3 mm. The maximum overall pump efficiency obtained was 51.76%, at 6000 rpm with a mass flow of 0.3 kg/s. Figure 9(b) presents the curves of power required as a function of flow rate at several rotational speeds. Again, higher power is required at higher rotational speeds and mass flow rates. The maximum power required was found to be 6888 W, for 6000 rpm and a mass flow rate of 2.3 kg/s.

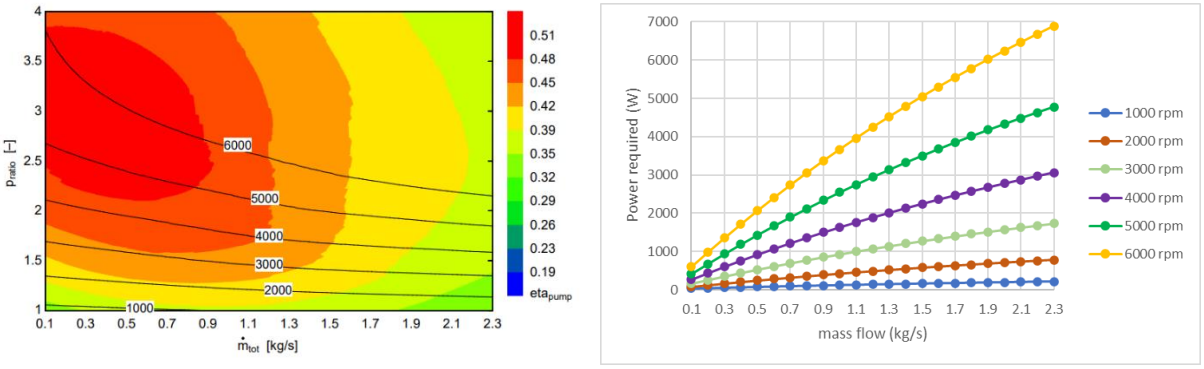

Figure 9: (a) Pressure ratio (black curves) and pump efficiency (colour map); (b) required power, as function of mass flow rate and rotational speed.

5 CONCLUSIONS

A complete design procedure for a Tesla pump was carried out in this work and its suitability to water and organic working fluids was assessed by evaluating the performance of a specifically designed pump working with water and with the extension of the analysis to R1233zd(E) and R1234yf working fluids. The key outcomes of the present work may be summarised as follows:

- An innovative model for the solution of the rotor flow field for a Tesla pump was developed. Starting from an existing literature approach on Tesla turbines (Talluri et al., 2018, Manfrida and Talluri 2019), the pump model was obtained, considering the real fluid behaviour.
- As an outcome of the developed model, a prototype was designed with water as a working fluid. The expected maximum efficiency achieved from the prototype is 26.8% with a rotational speed of 5000 rpm and a disc gap of 0.3 mm.
- The model was finally extended to organic working fluids, the results showed that relatively high pump efficiency can be reached for low mass flow rates and relatively high-pressure ratio. Both R1233zd(E) and R1234yf fluids achieved pump efficiencies above 50%.

As a final remark, the here conducted analysis showed how the complete assessment of a Tesla pump needs to take into account not only the rotor model, which is the main part discussed in the literature but also all the other components of the pump, especially the volute. Indeed, The most critical issue of the Tesla pump is its low efficiency. In order to increase its performance and to not lose its advantages, some interesting aspects should be developed in proper future works. The design of the discs could be improved, studying the performance with various discs' roughness or with the introduction of ribbed discs. Another improvement could be achieved through further assessing the volute design with a computational fluid dynamic analysis (CFD) in order to properly define the flow path inside the volute. Finally, experimental investigation of the Tesla pump with organic fluids and CO2 seems to still be missing in the literature.

REFERENCES

Alonso DH., Nogueira de Sà LF, Saen JSR, Silva ECN, 2019, Topology optimization based on a two-dimensional swirl flow model of Tesla-type pump devices, Computer and Mathematics with Applications, 77: p. 2499-2533.

Brun K., Friedman P., Dennis R., 2017, Fundamentals and Applications of Supercritical Carbon Dioxide (sCO_2) Based Power Cycle, Woodhead Publishing.

Foster M., 2006, The potential of a Tesla type device as a non pulsatile blood pump, Middlesex University of London, 2006.

J. Pacello, P. Hanas, 2000, Disc pump-type pump technology for hard-to-pump applications, Proceedings of the 17th international pump users symposium, Texas.

L. Dodsworth, "Operational Parametric Study of a Prototype Tesla Pump", Dalhousie University, Halifax, Nova Scotia, April 2016.

Manfrida G., Talluri L., 2019, Fluid dynamics assessment of the Tesla turbine rotor, Thermal Science.

Rice W., 1963, An analytical and experimental investigation of multiple disk pumps and compressors, J. Eng. Power, 85(3): p. 191-198

Talluri L., Fiaschi D., Neri G., Ciappi L., 2018, Design and optimization of a Tesla turbine for ORC applications, Applied Energy, 226(15): p. 300-319.

Van den Braembussche R.A., 2006, Flow and loss mechanism in volutes of centrifugal pumps, Von Karman Institute for Fluid Dynamics.